IEEE Sensors Council

# Robust Beamforming Design for Integrated Sensing and Communication Systems

Yongjun Xu, *Senior Member, IEEE*, Na Cao, Yi Jin, Haibo Zhang, Chongwen Huang, *Member, IEEE*, Qianbin Chen, *Senior Member, IEEE*, and Chau Yuen, *Fellow, IEEE*

***Abstract*—Integrated sensing and communication (ISAC) can improve spectral, energy, and transmission efficiency. To overcome the impact of channel uncertainties, we investigate a robust beamforming design problem for a multiple-input single-output based ISAC system with imperfect channel state information (CSI), where a multiantenna base station (BS) serves multiple wireless users and obtains state information of a point target. Based on bounded CSI error models, a total throughput maximization problem is formulated under the constraints of the minimum rate threshold of each communication user, sensing performance based on Cramér–Rao lower bound thresholds, and the maximum transmit power of the BS. The formulated problem with parameter perturbations belongs to a nonconvex one that is challenging to solve. To address this complexity, an iterative robust beamforming algorithm is designed by employing S-procedure, semidefinite relaxation technique, Schur complementarity conditions, and successive convex approximation. Simulation results demonstrate that the proposed algorithm exhibits better convergence and stronger robustness.**

***Index Terms*—Integrated sensing and communication (ISAC), robust beamforming, throughput maximization.**

## Nomenclature

| | |
|---|---|
| ISAC | Integrated sensing and communication. |
| BS | Base station. |
| RCC | Radar communication coexistence. |
| DFRC | Dual-function radar communication. |
| LFM | Linear frequency modulation. |
| PSK | Phase-shift keying. |
| CPM | Continuous phase modulation. |
| SF | Step frequency. |
| OFDM | Orthogonal frequency division multiplexing. |
| MIMO | Multiple-input multiple-output. |
| MUSIC | Multiple signal classification. |
| SINR | Signal-to-interference-plus-noise ratio. |
| CRLB | Cramér–Rao lower bound. |
| SCA | Successive convex approximation. |
| CSI | Channel state information. |
| MISO | Multiple-input single-output. |
| SDR | Semidefinite relaxation. |

## I. Introduction

With the growing number of communication users and the rising demand for various sensing services, spectrum resources have become exceptionally congested. Moreover, the mutual interference between terminals has pushed the corresponding performance close to theoretical limits [1], [2], [3]. To address these challenges, integrated sensing and communication (ISAC) has surfaced as a cost-effective solution, injecting new momentum to tackle the issues at hand. Specifically, the objective of ISAC is to tightly integrate sensing and wireless communication by sharing spectrum, hardware platforms, and signal processing frameworks, aiming for performance equilibrium and maximizing gains [4], [5], [6]. ISAC significantly enhances both spectrum and energy efficiency, concurrently curbing hardware costs and system power consumption.

Currently, ISAC systems are broadly classified into radar communication coexistence and dual-function radar communication (DFRC). The former employs separate waveforms, enhancing spectrum utilization by sharing communication and radar spectrum resources with minimal modifications required for existing hardware facilities [7], [8], [9]. However, its implementation requires clever design of transmission waveforms for both communication and radar to effectively control interference, leading to a higher level of signal processing complexity [10], [11]. In contrast, DFRC employs the same transmitter to produce dual-function waveforms in the same frequency band, significantly improving spectrum efficiency while reducing the

Manuscript received 14 March 2024; revised 27 May 2024; accepted 18 June 2024. Date of publication 2 July 2024; date of current version 22 July 2024. This work was supported in part by the National Natural Science Foundation of China under Grant U23A20279 and Grant 62271094, in part by the Natural Science Foundation of Chongqing under Grant CSTB2022NSCQ LZX0009 and Grant CSTB2023NSCQ-LZX0079, and in part by the Science and Technology Research Program of Chongqing Municipal Education Commission under Grant KJZD-K202200601. Recommended by Lead Guest Editor Fan Liu and Guest Editor Yuanhao Cui. *(Corresponding author: Yongjun Xu.)*

Yongjun Xu, Na Cao, Haibo Zhang, and Qianbin Chen are with the School of Communications and Information Engineering, Chongqing University of Posts and Telecommunications, Chongqing 400065, China (e-mail: xuyj@cqupt.edu.cn; s220101004@stu.cqupt.edu.cn; zhanghb@cqupt.edu.cn; chenqb@cqupt.edu.cn).

Yi Jin is with the China Academy of Space Technology-Xi'an, Xi'an 710100, China (e-mail: john.0216@163.com).

Chongwen Huang is with the Information Communication and Network Engineering, Zhejiang University, Hangzhou 310027, China (e-mail: chongwenhuang@zju.edu.cn).

Chau Yuen is with the School of Electrical and Electronics Engineering, Nanyang Technological University, Singapore 639798 (e-mail: chau.yuen@ntu.edu.sg).

Digital Object Identifier 10.1109/JSAS.2024.3421391

complexity of signal processing [12], [13]. Nevertheless, the DFRC system still presents several key issues that require further exploration, such as how to design waveforms to balance communication and radar sensing functionalities.

## A. Related Works

Therefore, more and more scholars have started to work on the waveform design for realizing ISAC systems. Based on the existing works, the literature review on waveform design in ISAC systems can be classified into the following three types.

*1) Sensing-Centric Waveform Design:* Sensing-centric waveform design aims to fully utilize existing sensing waveforms to simultaneously implement additional communication functions. As sensing waveforms typically do not directly carry modulation information, a common approach is to embed signaling information into the sensing waveforms, thus realizing both communication and sensing functions [14], [15], [16], [17], [18], [19], [20], [21], [22]. Specifically, Xie and Luo [14] proposed a design approach to modulate minimum frequency-shift keying signals onto linear frequency modulation (LFM) pulses. They discussed the relationship between signal power leakage and modulation data when the radar receiver bandwidth approximated the transmission signal bandwidth, and a method was suggested to eliminate power leakage by abandoning a certain channel capacity. However, the use of low-order modulation resulted in a relatively lower communication rate. In addition, modulating communication data into LFM signals using phase-shift keying (PSK) to achieve integrated waveforms is also an area of interest for researchers [15], [16]. Because PSK-LFM exhibits excellent constant-envelope characteristics, enabling efficient utilization of high-power amplifiers to generate integrated signals without causing significant nonlinear distortion. In [17], researchers devised an LFM signal based on continuous phase modulation (CPM) to address the issue of low spectral efficiency caused by the discontinuity in the phase of PSK-LFM. In [18] and [19], low-density parity-check codes and precoding techniques were, respectively, employed to design CPM-LFM waveforms, further enhancing spectral efficiency. However, the above single-carrier waveform design approaches struggle to achieve high data rates and bandwidth utilization while maintaining perceptual performance. Therefore, Han et al. [20] proposed a method based on step frequency (SF). SF signals are easy to generate and can provide large bandwidth and high resolution [21]. Nonetheless, ensuring radar performance remains unaffected by communication data proves challenging. To address these issues, Gaglione et al. [22] introduced pseudorandom sequences to improve spectral efficiency and reduce interdevice interference.

*2) Communication-Centric Waveform Design:* Orthogonal frequency division multiplexing (OFDM) has gained widespread application in the field of communication due to its advantages, such as resistance to multipath fading, high modulation efficiency, and wide bandwidth. It has also become a significant topic in the research on ISAC shared waveform design [23], [24], [25], [26], [27], [28], [29]. Liu et al. [23] proposed an ISAC system based on OFDM. By compensating and decohering the echoed information, they utilized subspace projection to achieve high-resolution joint estimation of target distance and velocity. Moreover, Yang et al. [24] utilized dynamic constellation expansion to adjust the positions of constellation points, reducing the probability of co-phase occurrence and consequently lowering the peak-to-average power ratio of OFDM. Since random communication information on different subcarriers may affect the ambiguity function, thereby diminishing sensing performance, Watabe et al. [25] proposed using precoding to ensure that communication information between different channels exhibits good autocorrelation and cross-correlation, thus mitigating the impact of communication on sensing. In addition, Hassanien et al. [26] implemented an ISAC system integrating multiple-input multiple-output (MIMO) and OFDM, which utilized the primary lobe of the beam emitted by the MIMO radar for target sensing and the side lobes for communication. Moreover, the authors in [27] and [28] employed diverse weighted vectors for phase modulation. In the aforementioned two ISAC systems, a communication symbol is represented by multiple radar pulses, resulting in a relatively lower communication rate, and only enabling radar-ranging functionality. In [29], an analysis was conducted on the periodogram and multiple signal classification (MUSIC) radar signal processing algorithm, aimed at improving radar resolution accuracy. Simulation results demonstrated that MUSIC is more suitable for high signal-to-interference-plus-noise ratio (SINR) scenarios, whereas the periodogram method is better suited for low SINR scenarios.

*3) Joint Waveform Design and Optimization:* In communication-centric design and sensing-centric design, the performance of sensing and communication may not be optimal. Therefore, it is essential to explore joint design approaches that are independent of existing radar or communication waveforms, which not only allows for accurate sensing while communicating at high rates but also provides additional freedom and flexibility [30]. To this end, various joint waveform designs have been proposed for ISAC systems [31], [32], [33], [34], [35], [36], [37], [38]. Elbir and Mishra [31] focused on designing a sparse array with hybrid beamforming for ISAC systems, and proposed a modeling and learning-based approach to jointly address the design of sparse arrays and hybrid ISAC beamforming. In comparison to the single communication user model established in [31], Grossi et al. [32] proposed a more complex multiuser multisensing target model, and applied a cognition-based design method, exploring the energy-efficient optimization problem in MIMO radar-communication spectrum sharing scenarios. Through simulation verification, the proposed method maximizes efficiency while ensuring sensing performance, although the beamforming vector is not optimized. Liu et al. [33] studied high-efficiency waveform design for ISAC systems, aiming to enhance system efficiency while guaranteeing target estimation performance. Under power budget and Cramér–Rao lower bound (CRLB) constraints, the efficiency of the transmit waveform has been maximized. To address the highly nonconvex fractional-order objective function involved in the proposed problem, the

Dinkelbach algorithm is introduced in [33]. Liu et al. [34] introduced the successive convex approximation (SCA) algorithm to more efficiently calculate results based on previous work. Simulation results demonstrated a significant improvement in iteration speed and efficiency performance compared with the algorithm proposed in [33]. Chen et al. [35] suggested maximizing sensing accuracy by minimizing the mean square error between the ideal beamforming and the actual beamforming, and derived a closed-form solution for a single communication user scenario. Furthermore, the simulation proves that the shared antenna deployment mode in ISAC systems achieves higher sensing accuracy and overall performance than the separate antenna deployment mode. Liu et al. [36] categorized sensing targets into point targets and extended targets, and guaranteed SINR for each communication user while minimizing CRLB. In addition, Qiu et al. [37] demonstrated the equivalence between CRLB and mean square error in the case of extended targets. In [38], the radar SINR maximization problem was first constructed to jointly optimize the beamforming and transmit signal matrices under power and modulus constraints, using alternating optimization and gradient projection algorithms to solve the problem efficiently.

### B. Motivations and Contributions

Although joint waveform design brings significant performance improvements to ISAC systems, even exponentially increasing spectral efficiency, achieving perfect channel state information (CSI) estimation remains challenging and impractical in actual communication systems due to diverse factors, such as noise, signal attenuation, and multipath propagation. Therefore, the previous works with perfect CSI [31], [32], [33], [34], [35], [36], [37], [38] may not be effective in actual systems, and they may introduce higher outages or message transmission errors. As a result, to limit the effects of channel uncertainty on the performance of ISAC systems in actual radio environments, it is necessary to consider the robust beamforming design.

Furthermore, the majority of the existing works [14], [15], [16], [17], [18], [19], [20], [21], [22], [23], [24], [25], [26], [27], [28], [29], [30], [31], [32], [33], [34], [35], [36], [37], [38] have concentrated on ISAC waveform design from different aspects. However, the system performance of sensing-centric [14], [15], [16], [17], [18], [19], [20], [21], [22] or communication-centric [23], [24], [25], [26], [27], [28], [29] designs is severely constrained by hardware platforms and signal processing algorithms. Achieving a favorable performance tradeoff between communication and sensing remains elusive. The main contributions are summarized as follows.

1) We propose a joint beamforming design framework for downlink multiple-input single-output (MISO) ISAC systems considering imperfect CSI for point target sensing and multiuser communications. The sensing performance is guaranteed while maximizing the system throughput to improve the overall system performance.
2) Due to infinite constraints caused by the imperfect CSI, the complex maximization throughput problem is a nonconvex difficult one. First, we transform the original problem into a convex one by applying Schur complementary condition, SCA technique, S-procedure, semidefinite relaxation (SDR) technique, and variable substitution methods. Then, the transformed problem becomes amenable to a solution using the CVX toolbox. Finally, an SCA algorithm is proposed.
3) Simulation results demonstrate the convergence and robustness of our proposed SCA algorithm. Specifically, it exhibits better convergence and achieves a 7.3% reduction in outage probability compared with the nonrobust algorithm.

### C. Organization and Notations

The rest of this article is organized as follows. Section II introduces the downlink MISO-ISAC system model and problem formulation. An iterative-based SCA algorithm is designed in Section III. Section IV gives the simulation results. Finally, Section V concludes this article.

*Notations:* Vectors and matrices are denoted by boldface lowercase letters and boldface uppercase letters, respectively. $\boldsymbol{A}^T$, $\boldsymbol{A}^H$, $\mathrm{rank}(\boldsymbol{A})$, $\mathrm{Tr}(\boldsymbol{A})$, and $\|\boldsymbol{A}\|_F$ denote the transpose, Hermitian conjugate transpose, rank, trace, and Frobenius norm of matrix $\boldsymbol{A}$, respectively. $\boldsymbol{A} \succeq \mathbf{0}$ indicates a positive semidefinite matrix. $\mathcal{CN}(\mu, \delta^2)$ denotes the Gaussian distributions with mean $\mu$ and variance $\delta^2$. $\mathbb{E}\{\cdot\}$ denotes the expectation operation. $\mathbb{C}^{M\times N}$ denotes an $M \times N$ dimensional complex matrix. $\|\boldsymbol{a}\|$ and $|\cdot|$ denote the Euclidean norm of $\boldsymbol{a}$ and the absolute operation, respectively. $\mathrm{Re}\{\cdot\}$ denotes the real part of a complex number. The abbreviations used in this article are given in the Nomenclature.

## II. System Model and Problem Formulation

As shown in Fig. 1, we consider a multiuser downlink MISO-ISAC system. Specifically, a BS equipped with $N$ antennas serves $K$ single-antenna users while obtaining state information of a point target. Without loss of generality, assuming $K < N$ [39]. Besides, we define $L$ as the communication frame length, $\forall k \in \mathcal{K} = \{1, 2, \ldots, K\}$ and $\forall l \in \mathcal{L} = \{1, 2, \ldots, L\}$ denote the sets of communication users and discrete-time indexes. $\mathbf{s}(l) = [s_1(l), s_2(l), \ldots, s_K(l)]^T \in \mathbb{C}^{K\times 1}$ denotes the vector of data sent to $K$ users at discrete time $l$, satisfying $\frac{1}{L}\sum_{l=1}^{L}\mathbf{s}(l)\mathbf{s}(l)^H = \boldsymbol{I}_{K\times K}$.

Based on the above analysis, the transmitted signal at discrete time $l$ of the BS can be formulated as [10]

$$\boldsymbol{x}(l) = \boldsymbol{W}\boldsymbol{s}(l) \tag{1}$$

where $\boldsymbol{W} = [\boldsymbol{w}_1, \boldsymbol{w}_2, \ldots \boldsymbol{w}_K] \in \mathbb{C}^{N\times K}$ denotes the beamforming vector sent by the BS. Therefore, the covariance matrix of $\boldsymbol{x}(l)$ can be expressed as

$$\boldsymbol{R}_x = \mathbb{E}\left\{\boldsymbol{x}(l)\boldsymbol{x}^H(l)\right\} = \boldsymbol{W}\boldsymbol{W}^H. \tag{2}$$

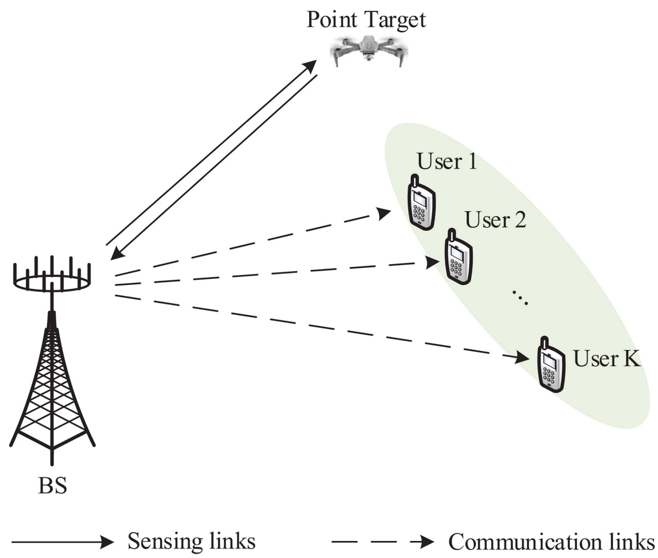


Fig. 1. MISO-ISAC system.

### A. Communication Models and Performance Metrics

The received signal by the communication user $k$ can be expressed as

$$y_k(l) = \boldsymbol{h}_k^H \boldsymbol{w}_k s_k(l) + \sum_{j=1, j\neq k}^{K} \boldsymbol{h}_k^H \boldsymbol{w}_j s_j(l) + n_k(l) \quad (3)$$

where $\boldsymbol{h}_k \in \mathbb{C}^{N\times 1}$ denotes the channel vector from the BS to the $k$th user, and $n_k(l) \sim \mathcal{CN}(0, \sigma_k^2)$ denotes the additive Gaussian white noise at the user $k$ with mean 0 and variance $\sigma_k^2$. Based on (3), the SINR of the user $k$ can be formulated by

$$\gamma_k = \frac{\left|\boldsymbol{h}_k^H \boldsymbol{w}_k\right|^2}{\sum_{j=1, j\neq k}^{K} \left|\boldsymbol{h}_k^H \boldsymbol{w}_j\right|^2 + \sigma_k^2}. \quad (4)$$

According to (4), the normalized throughput of the user $k$ can be expressed as

$$R_k = \log_2 \left(1 + \gamma_k\right). \quad (5)$$

### B. Sensing Models and Performance Metrics

Motivated by the authors in [41] and [42], it is reasonable for the communication signal sent by the dual-function BS to be used for sensing. Specifically, radar sensing does not require the transmission of valid information to accomplish its task. As long as the transmitted signal can interact with the target, the BS can process the target's echo signals to obtain target information and complete the sensing task. Therefore, by transmitting $\boldsymbol{x}(l)$, the echo signal at discrete time $l$ can be expressed as

$$\boldsymbol{y}_s(l) = \alpha \boldsymbol{a}(\theta) \boldsymbol{a}^H(\theta) \boldsymbol{x}(l) + n_s(l) \quad (6)$$

where $\boldsymbol{a}(\theta) = [1, e^{j2\pi\Delta \sin(\theta)}, \ldots, e^{j2\pi(N-1)\Delta\sin(\theta)}]^T \in \mathbb{C}^{N\times 1}$ denotes the steering vector for the transmitting antennas of the BS, and $\Delta$ denotes the normalized spacing between neighboring antennas. Similarly, $\boldsymbol{a}^H(\theta)$ denotes the steering vector of the receiving antennas. $\alpha \in \mathbb{C}$ represents the complex amplitude proportional to the radar cross section of the target and the round-trip path loss. $n_s(l) \sim \mathcal{CN}(0, \sigma_s^2)$ denotes the additive Gaussian white noise with mean 0 and variance $\sigma_s^2$ at the BS receiver.

CRLB can theoretically provide a minimum bound on the variance of the unbiased estimator, making it a valuable performance metric for target estimation. For the point target in an ISAC system, we obtain the position information of the target by estimating its relative angle $\theta$ with respect to the BS. Defining $\boldsymbol{A}(\theta) = \mathbf{a}(\theta)\mathbf{a}^H(\theta)$ as the total steering vector, according to work [43], the CRLB of $\theta$ can be expressed as follows (i.e., at the top of the page 5), where $\dot{\boldsymbol{A}}(\theta)$ denotes the derivative of $\boldsymbol{A}(\theta)$ (7) shown at the bottom of the next page.

### C. Robust Problem Formulation

Due to user mobility and the complexity of the electromagnetic environment, it becomes challenging to accurately obtain the CSI between the BS and users. Thus, assuming imperfect channel gains is a reasonable consideration,[1] as motivated by models of bounded CSI errors [46], we have

$$\mathcal{R}_h = \left\{\Delta \boldsymbol{h}_k \mid \boldsymbol{h}_k = \bar{\boldsymbol{h}}_k + \Delta\boldsymbol{h}_k : \|\Delta\boldsymbol{h}_k\|_2 \leq \zeta_k\right\} \quad (8)$$

where $\mathcal{R}_h$ denotes the set of tightly convex uncertainties, $\bar{\boldsymbol{h}}_k$ denotes the channel estimation vector, $\Delta\boldsymbol{h}_k$ denotes the corresponding channel estimation error, and $\zeta_k \geq 0$ denotes the upper bound,[2] on the parameters of uncertainty.

Therefore, the robust beamforming problem for the ISAC system can be formulated as

$$\begin{aligned} \mathbf{P}_1: \quad & \max_{\boldsymbol{w}_k} \; R_{\text{sum}}\left(\Delta\boldsymbol{h}_k\right) \\ \text{s.t.} \quad & \text{C1}: \text{CRLB}(\theta) \leq \beta \\ & \text{C2}: \|\boldsymbol{W}\|_F^2 \leq P^{\max} \\ & \text{C3}: R_k\left(\Delta\boldsymbol{h}_k\right) \geq R_k^{\min} \\ & \text{C4}: \Delta\boldsymbol{h}_k \in \mathcal{R}_h \end{aligned} \quad (9)$$

where $R_{\text{sum}} = \sum_{k=1}^{K} R_k$ denotes the total throughput of the system, $\beta$ denotes the threshold of CRLB, $P^{\max}$ denotes the maximum transmit power threshold of the BS, and $R_k^{\min}$ denotes the minimum transmission rate threshold of the communication user $k$, and constraint C1 is to ensure the sensing performance, C2 denotes the maximum transmit power constraint, C3 denotes the minimum transmission rate constraint of the communication user $k$, and C4 denotes the set of tightly convex uncertaintie.

Obviously, problem $\mathbf{P}_1$ is complicated and difficult to solve due to the following three aspects.

1) The total throughput in the objective function is nonconvex and NP-hard.
2) The nature of the Fisher information matrix causes constraint C1 to be nonconvex.
3) Constraint C3 contains an infinite number of dimensional nonconvex constraints.

[1] For the channel estimation phase, we can use the traditional channel estimation method to obtain the estimated channel values [44], [45].

[2] In practice, the values of upper bounds depend on the coherence time of the associated channel, the specific channel estimation schemes, and the time between channel estimation and packet transmission [47].

Therefore, we propose the SCA algorithm to solve problem $\mathbf{P}_1$.

## III. Robust Beamforming Problem Optimization

### A. Proposed SCA Algorithm

It is observed that the objective function and constraint C3 in problem $\mathbf{P}_1$ involve channel errors. In order to deal with it, an auxiliary variable $t$ is introduced, and based on the variable relaxation method, problem $\mathbf{P}_1$ can be reformulated as

$$\begin{aligned} \mathbf{P}_2 :\quad & \max_{\boldsymbol{w}_k, t}\ t \\ \text{s.t.}\quad & \text{C5} : R_{\text{sum}}\left(\Delta \boldsymbol{h}_k\right) \geq t \\ & \text{C1} \sim \text{C4}. \end{aligned} \tag{10}$$

Problem $\mathbf{P}_2$ remains a challenging nonconvex optimization problem, and to deal with the channel uncertainty as well as the nonconvexity in constraints C3 and C5, the following variational relaxation is considered:

$$\frac{\phi_k}{\chi_k} \geq 2^{r_k} - 1 \tag{11}$$

$$\phi_k \leq \left|\boldsymbol{h}_k^H \boldsymbol{w}_k\right|^2 \tag{12}$$

$$\chi_k \geq \sum_{j=1, j\neq k}^{K} \left|\boldsymbol{h}_k^H \boldsymbol{w}_j\right|^2 + \sigma_k^2 \tag{13}$$

where $\phi_k$, $\chi_k$, and $r_k$ are the introduced slack variables. However, (11) is still nonconvex, and in order to transform it into a convex one, we apply Taylor series expansion method, then (11) can be approximately linearized as follows:

$$\begin{cases} \phi_k \geq \mathrm{e}^{x_k^1}, x_k^1 - x_k^2 \geq x_k^3 \\ \chi_k \leq \mathrm{e}^{\bar{x}_k^2}\left(x_k^2 - \bar{x}_k^2 + 1\right) \\ 2^{r_k} - 1 \leq \mathrm{e}^{\bar{x}_k^3}\left(x_k^3 - \bar{x}_k^3 + 1\right) \end{cases} \tag{14}$$

where $x_k^1$, $x_k^2$, and $x_k^3$ are slack variables, respectively, and $\bar{x}_k^2$ and $\bar{x}_k^3$ are the values of the last iteration of $x_k^2$ and $x_k^3$, respectively. Defining $\boldsymbol{W}_k = \boldsymbol{w}_k \boldsymbol{w}_k^H$, and satisfying $\boldsymbol{W}_k \succeq \mathbf{0}$, $\text{Rank}(\boldsymbol{W}_k) = 1$. According to (8), (12) can be rewritten as

$$\begin{aligned} \phi_k \leq\ & \Delta \boldsymbol{h}_k^H \boldsymbol{B}_1 \Delta \boldsymbol{h}_k + 2\,\text{Re}\left\{\bar{\boldsymbol{h}}_k^H \boldsymbol{B}_1 \Delta \boldsymbol{h}_k\right\} \\ & + \bar{\boldsymbol{h}}_k^H \boldsymbol{B}_1 \bar{\boldsymbol{h}}_k,\ \|\Delta \boldsymbol{h}_k\|_2^2 \leq \zeta_k^2. \end{aligned} \tag{15}$$

Similarly, (13) can be rewritten as

$$\begin{aligned} \chi_k \geq\ & \Delta \boldsymbol{h}_k^H \boldsymbol{B}_2 \Delta \boldsymbol{h}_k + 2\,\text{Re}\left\{\bar{\boldsymbol{h}}_k^H \boldsymbol{B}_2 \Delta \boldsymbol{h}_k\right\} \\ & + \bar{\boldsymbol{h}}_k^H \boldsymbol{B}_2 \bar{\boldsymbol{h}}_k + \sigma_k^2, \|\Delta \boldsymbol{h}_k\|_2^2 \leq \zeta_k^2 \end{aligned} \tag{16}$$

where $\boldsymbol{B}_1 = \boldsymbol{W}_k$ and $\boldsymbol{B}_2 = \sum_{j=1, j\neq k}^{K} \boldsymbol{W}_j$. To address the channel uncertainties arising from parameter perturbations in (15) and (16), we introduce Lemma 1 to deal with it.

*Lemma 1 (S-procedure [48]):* Define the quadratic functions $f_i(\boldsymbol{x}) = \boldsymbol{x}^H \boldsymbol{A}_i \boldsymbol{x} + 2\text{Re}\{\boldsymbol{b}_i^H \boldsymbol{x}\} + c_i, i = \{1, 2\}$, where $\boldsymbol{A}_i \in \mathbb{C}^{N\times N}$, $\boldsymbol{b}_i \in \mathbb{C}^{N\times 1}$, $\boldsymbol{x} \in \mathbb{C}^{N\times 1}$, and $c_i \in \mathbb{R}$. The condition $f_1(\boldsymbol{x}) \leq 0 \Rightarrow f_2(\boldsymbol{x}) \leq 0$ holds if and only if there exists $\lambda \geq 0$ such that

$$\lambda \begin{bmatrix} \boldsymbol{A}_1 & \boldsymbol{b}_1 \\ \boldsymbol{b}_1^H & c_1 \end{bmatrix} - \begin{bmatrix} \boldsymbol{A}_2 & \boldsymbol{b}_2 \\ \boldsymbol{b}_2^H & c_2 \end{bmatrix} \succeq \mathbf{0}. \tag{17}$$

Defining an auxiliary variable $\lambda_1 \geq 0$, according to Lemma 1, the semiinfinite dimensional constraint (15) can be transformed into the following linear matrix inequality:

$$\begin{bmatrix} \boldsymbol{B}_1 + \lambda_1 \boldsymbol{I}_{N\times N} & \boldsymbol{B}_1 \bar{\boldsymbol{h}}_k \\ \bar{\boldsymbol{h}}_k^H \boldsymbol{B}_1 & \bar{\boldsymbol{h}}_k^H \boldsymbol{B}_1 \bar{\boldsymbol{h}}_k - \phi_k - \lambda_1 \zeta_k^2 \end{bmatrix} \succeq \mathbf{0}. \tag{18}$$

*Proof:* See Appendix. Similarly, defining $\lambda_2 \geq 0$ as an auxiliary variable, (16) can be transformed into the following form:

$$\begin{bmatrix} -\boldsymbol{B}_2 + \lambda_2 \boldsymbol{I}_{N\times N} & -\boldsymbol{B}_2 \bar{\boldsymbol{h}}_k \\ -\bar{\boldsymbol{h}}_k^H \boldsymbol{B}_2 & -\bar{\boldsymbol{h}}_k^H \boldsymbol{B}_2 \bar{\boldsymbol{h}}_k - \sigma_k^2 + \chi_k - \lambda_2 \zeta_k^2 \end{bmatrix} \succeq \mathbf{0}. \tag{19}$$

Furthermore, to transform the nonconvex constraint C1 into a convex one, we employ Schur complement condition to convert it into a manageable form [49]. First, it is expressed equivalently as

$$\text{Tr}\left(\dot{\boldsymbol{A}}^H(\theta)\dot{\boldsymbol{A}}(\theta)\boldsymbol{R}_x\right) - D \geq \frac{\left|\text{Tr}\left(\dot{\boldsymbol{A}}^H(\theta)\boldsymbol{A}(\theta)\boldsymbol{R}_x\right)\right|^2}{\text{Tr}\left(\boldsymbol{A}^H(\theta)\boldsymbol{A}(\theta), \boldsymbol{R}_x\right)} \tag{20}$$

where $D = \sigma_s^2/2\beta|\alpha|^2 L$. Then, we use the Schur complement condition, (20) can be rewritten as

$$\begin{bmatrix} \text{Tr}\left(\dot{\boldsymbol{A}}^H(\theta)\dot{\boldsymbol{A}}(\theta)\boldsymbol{R}_x\right) - D & \text{Tr}\left(\dot{\boldsymbol{A}}^H(\theta)\boldsymbol{A}(\theta)\boldsymbol{R}_x\right) \\ \text{Tr}\left(\boldsymbol{A}^H(\theta)\dot{\boldsymbol{A}}(\theta)\boldsymbol{R}_x\right) & \text{Tr}\left(\boldsymbol{A}^H(\theta)\boldsymbol{A}(\theta)\boldsymbol{R}_x\right) \end{bmatrix} \succeq \mathbf{0}. \tag{21}$$

Based on the above analysis, the original nonconvex optimization problem $\mathbf{P}_1$ can be reformulated as follows:

$$\begin{aligned} \mathbf{P}_3 :\quad & \max_{\boldsymbol{W}_k, t, \Sigma}\ t \\ \text{s.t.}\quad & \hat{\text{C}}1 : (21) \\ & \hat{\text{C}}2 : \sum_{k=1}^{K} \text{Tr}\left(\boldsymbol{W}_k\right) \leq P^{\max} \\ & \bar{\text{C}}3 : r_k \geq R_k^{\min} \\ & \text{C5} : (14), (18), (19) \\ & \text{C6} : \boldsymbol{W}_k \succeq \mathbf{0} \\ & \text{C7} : \text{Rank}\left(\boldsymbol{W}_k\right) = 1 \\ & \text{C8} : \lambda_1 \geq 0, \lambda_2 \geq 0 \end{aligned} \tag{22}$$

---

$$\text{CRLB}\left(\theta\right) = \frac{\sigma_s^2}{2\mid\alpha\mid^2 L} \times \frac{\text{Tr}(\boldsymbol{A}^H(\theta)\boldsymbol{A}(\theta)\boldsymbol{R}_x)}{\text{Tr}(\dot{\boldsymbol{A}}^H(\theta)\dot{\boldsymbol{A}}(\theta)\boldsymbol{R}_x)\text{Tr}(\boldsymbol{A}^H(\theta)\boldsymbol{A}(\theta)\boldsymbol{R}_x) - \mid \text{Tr}(\dot{\boldsymbol{A}}^H(\theta)\boldsymbol{A}(\theta)\boldsymbol{R}_x)\mid^2}. \tag{7}$$

**Algorithm 1:** Proposed SCA Algorithm.

1: **Initialize**: $N$, $K$, $L$, $\bar{\boldsymbol{h}}_k$, $\zeta_k$, $\beta$, $P^{\max}$, $R_k^{\min}$, $\bar{x}_k^{(0),2}$, $\bar{x}_k^{(0),3}$;
2: Set the initial iteration value $x = 1$, $\eta > 0$ as the convergence accuracy, and $X_{\max}$ as the maximum iteration number;
3: **while** $|R_{\text{sum}}^{(x)} - R_{\text{sum}}^{(x-1)}| \geq \eta$ or $x \leq X_{\max}$ **do**
4: Solve $\mathbf{P}_3$ with given $\bar{x}_k^{(x-1),2}$, $\bar{x}_k^{(x-1),3}$, and obtain the optimal solution denoted by $\bar{x}_k^{(x),2}$, $\bar{x}_k^{(x),3}$, $\{\boldsymbol{W}_k^{(x)}\}_{k=1}^K$;
5: **until** converges;
6: **if** Rank($\boldsymbol{W}_k^{(x)}$) == 1 **then**
7: $\boldsymbol{w}_k^{(x)}$ is obtained via the eigenvalue decomposition method;
8: **else**
9: $\boldsymbol{w}_k^{(x)}$ is obtained by using the singular value decomposition method [50];
10: **end if**
11: $x = x + 1$;
12: **end while**
13: **out put**: $\boldsymbol{w}_k^*$.

where $\Sigma = \{\phi_k, \chi_k, r_k, x_k^1, x_k^2, x_k^3, \lambda_1, \lambda_2\}$. Problem $\mathbf{P}_3$ is still nonconvex due to $\text{Rank}(\boldsymbol{W}_k) = 1$ in C6, we relax it based on the SDR method. Then, problem $\mathbf{P}_3$ becomes a complex convex one that can be solved directly using the CVX toolbox. Since the solution obtained in problem $\mathbf{P}_3$ by removing the constraints using the SDR method is only an upper bound on problem $\mathbf{P}_1$, a Gaussian randomization method is needed to approximate the near-optimal solution. We assume that the solution of the problem $\mathbf{P}_3$ is $\boldsymbol{W}_k^*$ with $\text{Rank}(\boldsymbol{W}_k^*) = 1$, then $\boldsymbol{w}_k^*$ can be obtained by eigenvalue decomposition; otherwise, $\boldsymbol{w}_k^*$ can be obtained by singular value decomposition [50]. Finally, the proposed iteration-based SCA algorithm is summarized in Algorithm 1.

### B. Convergence Analysis

To better analysis the convergence of Algorithm 1, we define $\boldsymbol{W}_k^{(x)}$ as the $x$th iteration solution of $\mathbf{P}_3$, $x$ as the iteration number, and $R_{\text{sum}}(\boldsymbol{W}_k) = \sum_{k=1}^K R_k$ as the total throughput of the system. According to step 3 of Algorithm 1, the following condition is satisfied:

$$R_{\text{sum}}(\boldsymbol{W}_k^{(x-1)}) \leq R_{\text{sum}}(\boldsymbol{W}_k^{(x)}) \tag{23}$$

it is observed that the final value of $R_{\text{sum}}(\boldsymbol{W}_k)$ either equals or surpasses the value obtained in the last iteration. Moreover, the cumulative throughput continues to increase within a defined range, thus confirming the convergence of Algorithm 1.

### C. Complexity Analysis

Based on the method in [51], the complexity of Algorithm 1 can be denoted as $O = \mathcal{O}(x_1(x_2 + x_3))$ with the following expression:

$$x_1 = \sqrt{K(8 + 3N)} \tag{24}$$

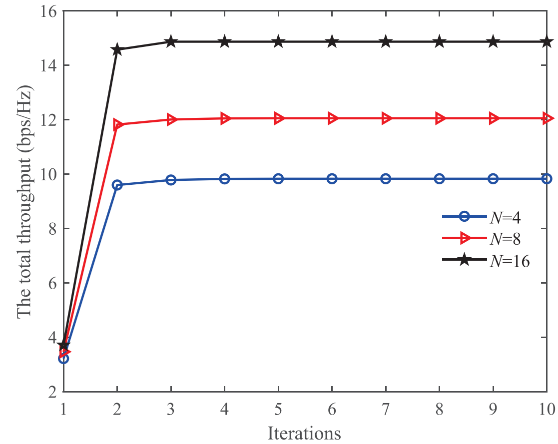


Fig. 2. Convergence of the proposed algorithm.

$$x_2 = n(6K + KN^3 + 2K(N+1)^3) \tag{25}$$

$$x_3 = n^2(6K + KN^2 + 2K(N+1)^2) \tag{26}$$

where $n = \mathcal{O}(KN^2)$ denotes the total number of elements to be optimized, $x_1$ denotes the number of iterations, and $x_2$ and $x_3$ denote the complexity of each iteration.

## IV. Simulation Results

In this section, the effectiveness of the proposed algorithm is evaluated by numeral simulations. The system channel fading model is assumed to be large-scale fading, and each individual channel fading model is independent, following the distribution: $Q = \psi d_i^{-\alpha}$, where $\psi = -30$ dB represents the path loss, $d_i$ represents the distance between any two devices, and $\alpha = 3$ denotes the path loss exponent [52]. Furthermore, it is assumed that the point target is at its $0^\circ$ position with respect to the dual-function BS. Without loss of generality, other parameters are defined as $\sigma_k = \sigma_s = 10^{-7}$ W, $P^{\max} = 5$ W, $R_k^{\min} = 0.1$ bps/Hz [53], $L = 30$, $K = 2$, $\beta = 0.025$ [54], $X_{\max} = 10^5$, and $\eta = 10^{-5}$. Define the normalized channel estimation errors as $\psi_h = \frac{\zeta_k}{\|\bar{\boldsymbol{h}}_{b,k}\|^2} = 0.1$.

Fig. 2 depicts the convergence of the proposed algorithm under different numbers of antennas $N$ at the BS. Clearly, the proposed algorithm tends to consistently converge after approximately five iterations, demonstrating strong convergence. In addition, the total system throughput increases with the growing $N$. This can be attributed to the larger $N$, which provides more degrees of freedom, enhancing signal coverage and transmission rates, thereby improving beamforming gain and overall system throughput.

Fig. 3 depicts the total system throughput versus the minimum rate threshold $R_k^{\min}$ under various channel error upper bounds $\zeta_k$. It is clear that for the same $\zeta_k$, the total system throughput increases with $R_k^{\min}$ when $R_k^{\min}$ is low. This is because the increased $R_k^{\min}$ compels the system to allocate more power to each user to meet the higher $R_k^{\min}$ requirements, thereby increasing the throughput per user. Furthermore, at the same $R_k^{\min}$, the total system throughput decreases with an increase

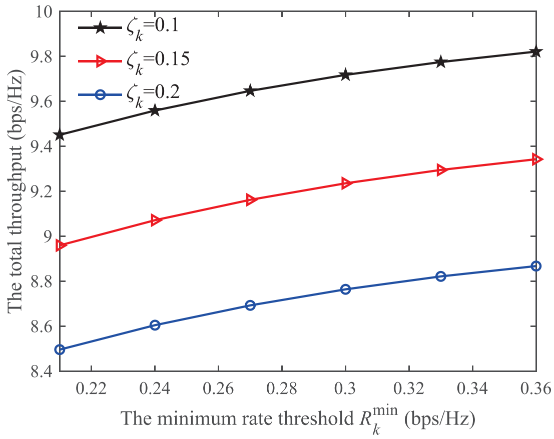


Fig. 3. Total throughput versus $R_k^{\min}$ under different $\zeta_k$.

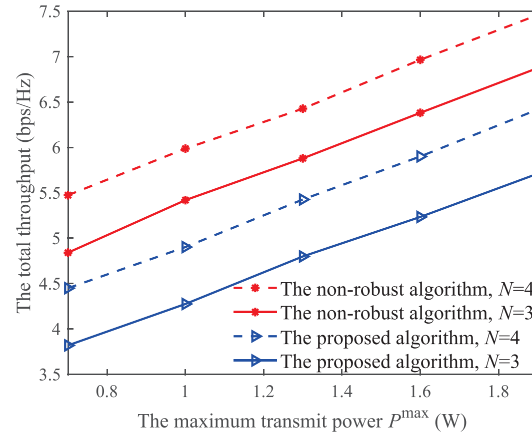


Fig. 5. Total throughput versus $P^{\max}$ under different algorithms.

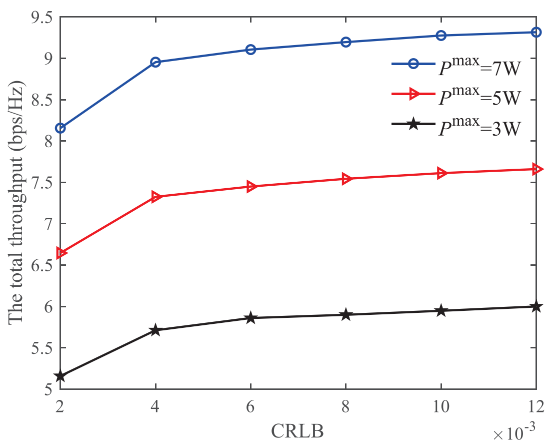


Fig. 4. Total throughput versus the CRLB under different $P^{\max}$.

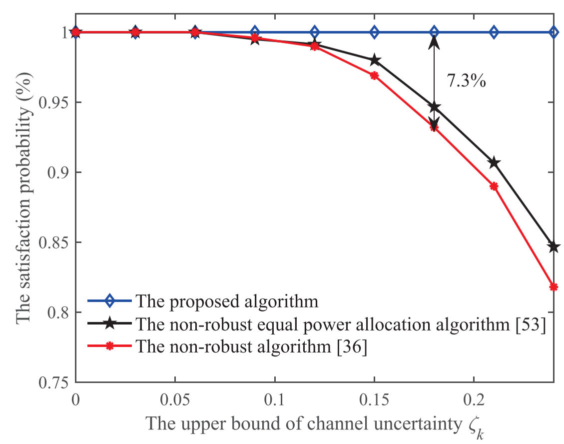


Fig. 6. Satisfaction probability versus $\zeta_k$ under different algorithms.

in $\zeta_k$. This is because the larger $\zeta_k$ indicates a higher channel estimation error and a more challenging channel environment, resulting in a reduction in the total system throughput.

Fig. 4 depicts the total system throughput versus the thresholds of CRLB under various maximum transmit powers $P^{\max}$. Obviously, the total system throughput exhibits an increasing trend with rising CRLB thresholds. This can be attributed to the inherent performance tradeoff between communication and sensing, given a specific $P^{\max}$. A larger CRLB threshold implies that the system demands less sensing accuracy. Consequently, less power is directed toward the point targets, allowing more power to be allocated to communication data transmission. This leads to an enhancement in communication performance and an overall increase in total throughput. Furthermore, while keeping the CRLB threshold constant, the total system throughput increases with higher $P^{\max}$. This is because the increased value of $P^{\max}$ expands the feasible domain of transmitted power, subsequently boosting the data rate.

Fig. 5 depicts the total system throughput versus the maximum transmit power $P^{\max}$ under two different algorithms. Evidently, the total system throughput of both algorithms increases with the increasing $P^{\max}$. This is because boosting $P^{\max}$ leads to stronger signals transmitted by the BS, making them less susceptible to interference or attenuation during transmission. Consequently, the receiving end can more easily decode the received signal, thereby enhancing the overall system throughput. The robust algorithm, as it ensures that the system operates normally in uncertain and noisy environments, typically incurs a cost of reducing the overall throughput to achieve higher stability and reliability. Furthermore, under the same $P^{\max}$, when $\zeta_k$ is small and $N$ is large, the total system throughput is also larger. This is attributed to the improvement in the channel environment and the increased beamforming gain, resulting in an overall increase in system throughput.

Fig. 6 depicts the probability of satisfaction (i.e., 1-outage probability) for various channel error upper bounds $\zeta_k$ under there distinct algorithms. Clearly, the proposed algorithm demonstrates a remarkable 100% probability of satisfaction, when $\zeta_k = 0.18$, compared to the nonrobust algorithm, its satisfaction probability is improved by 7.3%. This is because designing with bounded CSI errors ensures that even in the worst-case scenario, the system can still operate smoothly. In contrast, the satisfaction probabilities of nonrobust algorithm and nonrobust equal power allocation algorithms decrease as $\zeta_k$ increases. This is because CSI errors introduce discrepancies between system design and actual operation, leading to improper resource allocation and insufficient system robustness, thereby increasing the outage probability. In addition, the satisfaction probability of the nonrobust equal power allocation algorithm is higher than that of the nonrobust algorithm because the nonrobust equal power allocation algorithm is less sensitive to CSI errors, resulting in a higher satisfaction probability.

## V. Conclusion

In this article, we investigated a robust beamforming problem for a MISO-ISAC system with channel uncertainties. A nonconvex robust optimization problem for maximizing the total throughput was formulated by considering the minimum transmission rate constraint of each user, the sensing threshold constraint of the CRLB, and the maximum transmit power constraint. The original problem was transformed into the convex one by applying Schur complementary condition, SCA, S-procedure, SDR, and the variable substitution method. Simulation results demonstrated that the proposed algorithm exhibits better convergence and has a lower outage probability than the nonrobust algorithm.

## Appendix
## Proof of Lemma 1

*Proof:* For Lemma 1 to hold for $f_1(\boldsymbol{x}) \le 0 \Rightarrow f_2(\boldsymbol{x}) \le 0$ is equivalent to holding for $f_1(\boldsymbol{x}) \le 0$ if and only if there exists $\lambda \ge 0$ such that $\lambda f_1(\boldsymbol{x}) - f_2(\boldsymbol{x}) \ge 0$ holds. This can be written in the following quadratic matrix form:

$$\lambda \begin{bmatrix}\boldsymbol{x}^H & \boldsymbol{I}\end{bmatrix}\begin{bmatrix}\boldsymbol{A}_1 & \boldsymbol{b}_1 \\ \boldsymbol{b}_1^H & c_1\end{bmatrix}\begin{bmatrix}\boldsymbol{x} \\ \boldsymbol{I}\end{bmatrix} - \begin{bmatrix}\boldsymbol{x}^H & \boldsymbol{I}\end{bmatrix}\begin{bmatrix}\boldsymbol{A}_2 & \boldsymbol{b}_2 \\ \boldsymbol{b}_2^H & c_2\end{bmatrix}\begin{bmatrix}\boldsymbol{x} \\ \boldsymbol{I}\end{bmatrix} \ge \boldsymbol{0}$$

$$\Leftrightarrow \begin{bmatrix}\boldsymbol{x}^H & \boldsymbol{I}\end{bmatrix}\left\{\lambda \begin{bmatrix}\boldsymbol{A}_1 & \boldsymbol{b}_1 \\ \boldsymbol{b}_1^H & c_1\end{bmatrix} - \begin{bmatrix}\boldsymbol{A}_2 & \boldsymbol{b}_2 \\ \boldsymbol{b}_2^H & c_2\end{bmatrix}\right\}\begin{bmatrix}\boldsymbol{x} \\ \boldsymbol{I}\end{bmatrix} \ge \boldsymbol{0} \tag{27}$$

since the quadratic matrix (27) is nonnegative, we have

$$\lambda \begin{bmatrix}\boldsymbol{A}_1 & \boldsymbol{b}_1 \\ \boldsymbol{b}_1^H & c_1\end{bmatrix} - \begin{bmatrix}\boldsymbol{A}_2 & \boldsymbol{b}_2 \\ \boldsymbol{b}_2^H & c_2\end{bmatrix} \succeq \boldsymbol{0}. \tag{28}$$

Then, we give a proof for (18) [(19) will not be repeated]. Equations (8) and (15) can be written in quadratic form as follows:

$$\begin{cases} f_1(\boldsymbol{\Delta h}_k) = \Delta \boldsymbol{h}_k^H \Delta \boldsymbol{h}_k - \zeta_k^2 \le 0 \\ f_2(\boldsymbol{\Delta h}_k) = \phi_k - \Delta \boldsymbol{h}_k^H \boldsymbol{B}_1 \Delta \boldsymbol{h}_k - 2\mathrm{Re}\{\bar{\boldsymbol{h}}_k^H \boldsymbol{B}_1 \Delta \boldsymbol{h}_k\} \\ \qquad\qquad -\bar{\boldsymbol{h}}_k^H \boldsymbol{B}_1 \bar{\boldsymbol{h}}_k \le 0 \end{cases} \tag{29}$$

where $\boldsymbol{x} = \Delta \boldsymbol{h}_k$, $\boldsymbol{A}_1 = \boldsymbol{I}_{N\times N}$, $\boldsymbol{b}_1 = 0$, $c_1 = -\zeta_k^2$, $\boldsymbol{A}_2 = -\boldsymbol{B}_1$, $\boldsymbol{b}_2 = -\boldsymbol{B}_1\bar{\boldsymbol{h}}_k$, and $c_2 = -\bar{\boldsymbol{h}}_k^H \boldsymbol{B}_1 \bar{\boldsymbol{h}}_k + \phi_k$. According to Lemma 1, for $f_1(x) \le 0 \Rightarrow f_2(x) \le 0$ to hold, we have

$$\begin{bmatrix} \boldsymbol{B}_1 + \lambda_1 \boldsymbol{I}_{N\times N} & \boldsymbol{B}_1 \bar{\boldsymbol{h}}_k \\ \bar{\boldsymbol{h}}_k^H \boldsymbol{B}_1 & \bar{\boldsymbol{h}}_k^H \boldsymbol{B}_1 \bar{\boldsymbol{h}}_k - \phi_k - \lambda_1 \zeta_k^2 \end{bmatrix} \succeq \boldsymbol{0}. \tag{30}$$

The proof is complete.

## References


[1] F. Liu, C. Masouros, A. P. Petropulu, H. Griffiths, and L. Hanzo, "Joint radar and communication design: Applications, state-of-the-art, and the road ahead," *IEEE Trans. Commun.*, vol. 68, no. 6, pp. 3834–3862, Jun. 2020.

[2] Y. Xu, H. Xie, Q. Wu, C. Huang, and C. Yuen, "Robust max-min energy efficiency for RIS-aided HetNets with distortion noises," *IEEE Trans. Commun.*, vol. 70, no. 2, pp. 1457–1471, Feb. 2022.

[3] D. Li, "Hybrid active and passive antenna selection for backscatter-assisted MISO systems," *IEEE Trans. Commun.*, vol. 68, no. 11, pp. 7258-7269, Nov. 2020.

[4] F. Liu, C. Masouros, A. Li, T. Ratnarajah, and J. Zhou, "MIMO radar and cellular coexistence: A power-efficient approach enabled by interference exploitation," *IEEE Trans. Signal Process.*, vol. 66, no. 14, pp. 3681–3695, Jul. 2018.

[5] S. Lu et al., "Integrated sensing and communications: Recent advances and ten open challenges," *IEEE Internet Things J.*, vol. 11, no. 11, pp. 19094–19120, Jun. 2024.

[6] F. Dong, F. Liu, Y. Cui, S. Lu, and Y. Li, "Sensing as a service in 6G perceptive mobile networks: Architecture, advances, and the road ahead," *IEEE Netw.*, vol. 38, no. 2, pp. 87–96, Mar. 2024.

[7] L. Zheng, M. Lops, Y. C. Eldar, and X. Wang, "Radar and communication coexistence: An overview: A review of recent methods," *IEEE Signal Process. Mag.*, vol. 36, no. 5, pp. 85–99, Sep. 2019.

[8] J. Qian, M. Lops, L. Zheng, X. Wang, and Z. He, "Joint system design for coexistence of MIMO radar and MIMO communication," *IEEE Trans. Signal Process.*, vol. 66, no. 13, pp. 3504–3519, Jul. 2018.

[9] M. Rahman, J. A. Zhang, X. Huang, Y. J. Guo, and R. W. Heath, "Framework for a perceptive mobile network using joint communication and radar sensing," *IEEE Trans. Aerosp. Electron. Syst.*, vol. 56, no. 3, pp. 1926–1941, Jun. 2020.

[10] X. Liu, T. Huang, N. Shlezinger, Y. Liu, J. Zhou, and Y. C. Eldar, "Joint transmit beamforming for multiuser MIMO communications and MIMO radar," *IEEE Trans. Signal Process.*, vol. 68, pp. 3929–3944, 2020.

[11] F. Liu, L. Zhou, C. Masouros, A. Li, W. Luo, and A. Petropulu, "Toward dual-functional radar-communication systems: Optimal waveform design," *IEEE Trans. Signal Process.*, vol. 66, no. 16, pp. 4264–4279, Aug. 2018.

[12] P. Kumari and J. Choi, "IEEE 802.11 ad-based radar: An approach to joint vehicular communication radar system," *IEEE Trans. Veh. Technol.*, vol. 67, no. 4, pp. 3012–3027, Apr. 2018.

[13] W. Yuan, F. Liu, C. Masouros, J. Yuan, D. W. K. Ng, and N. González-Prelcic, "Bayesian predictive beamforming for vehicular networks: A low-overhead joint radar-communication approach," *IEEE Trans. Wireless Commun.*, vol. 20, no. 3, pp. 1442–1456, Mar. 2021.

[14] R. Xie and K. Luo, "Waveform design for LFM-MPSK-based integrated radar and communication toward IoT applications," *IEEE Internet Things J.*, vol. 9, no. 7, pp. 5128–5141, Apr. 2022.

[15] Y. Gu, L. Zhang, Y. Zhou, and Q. Zhang, "Embedding communication symbols into radar waveform with orthogonal FM scheme," *IEEE Sens. J.*, vol. 18, no. 21, pp. 8709–8719, Nov. 2018.

[16] Z. Lyu et al., "Radar-centric photonic terahertz integrated sensing and communication system based on LFM-PSK waveform," *IEEE Trans. Microw. Theory Techn.*, vol. 71, no. 11, pp. 5019–5027, Nov. 2023.

[17] F. Uysal, "Phase-coded FMCW automotive radar: System design and interference mitigation," *IEEE Trans. Veh. Technol.*, vol. 69, no. 1, pp. 270–281, Jan. 2020.

[18] Q. Li, K. Dai, Y. Zhang, and H. Zhang, "Integrated waveform for a joint radar-communication system with high-speed transmission," *IEEE Wireless Commun. Lett.*, vol. 8, no. 4, pp. 1208–1211, Aug. 2019.

[19] Y. Liu and T. Zao, "Novel radar and communication integration waveform based on shaped octal phase-shift keying modulation," *IEEE Wireless Commun. Lett.*, vol. 10, no. 2, pp. 353–367, Feb. 2021.

[20] T. Han, R. Senanayake, P. Smith, J. Evans, W. Moran, and R. Evans, "Combined radar and communications with phase-modulated frequency permutations," *IEEE Open J. Commun. Soc.*, vol. 4, pp. 967–989, Apr. 2023.

[21] S. Skarta, A. Hourant, and G. Hu, "Interference mitigation in automotive radars using pseudo-random cyclic orthogonal sequences," *IEEE Trans. Geosci. Remote Sens.*, vol. 19, no. 20, pp. 4459, Nov. 2019.

[22] D. Gaglione, C. Clemente, and R. Liu, "Waveform design for communicating radar systems using fractional Fourier transform," *IEEE Trans. Wireless Commun.*, vol. 18, no. 11, pp. 57–69, Jun. 2018.

[23] Y. Liu, G. Liao, and T. Yang, "Adaptive OFDM integrated radar and communications waveform design based on information theory," *IEEE Commun. Lett.*, vol. 21, no. 10, pp. 2174–2177, Oct. 2017.

[24] Y. Yang, J. Mei, and Y. Luo, "Research on reducing PAPR of QAM-OFDM radar-communication integration sharing signal," *IEEE Trans. Wireless Commun.*, vol. 11, no. 3, pp. 578–582, Mar. 2022.

[25] H. Watabe, T. Abe, and Y. Yamao, "On radar and communication integrated system using OFDM signal," *IEEE Trans. Veh. Technol.*, vol. 71, no. 3, pp. 3281–3286, Mar. 2022.

[26] A. Hassanien, M. G. Amin, Y. D. Zhang, and F. Ahmad, "Dual-function radar-communications: Information embedding using sidelobe control and waveform diversity," *IEEE Trans. Signal Process.*, vol. 64, no. 8, pp. 2168–2181, Apr. 2016.

[27] Z. Huang, C. Huang, and B. Tang, "Waveform design for dual-function radar communications based on the MIMO platform," *IEEE Trans. Veh. Technol.*, vol. 70, no. 8, pp. 7980–7991, Aug. 2021.

[28] A. C. F. Peterle, W. Costa, H. Camporez, M. Segatto, H. Rocha, and J. A. L. Silva, "Orthogonal chirp division multiplexing in visible light communication: A performance comparison with OFDM-based systems," *IEEE Trans. Commun.*, vol. 64, no. 9, pp. 3946–3957, Dec. 2016.

[29] L. Giroto et al., "Discrete-Fresnel domain channel estimation in OCDM-based radar systems," *IEEE Trans. Microw. Theory Techn.*, vol. 71, no. 5, pp. 2258–2275, May 2023.

[30] Z. Ren et al., "Fundamental CRB-rate tradeoff in multi-antenna ISAC systems with information multicasting and multi-target sensing," *IEEE Trans. Wireless Commun.*, vol. 23, no. 4, pp. 3870–3885, Apr. 2024.

[31] A. Elbir and K. Mishra, "Deep sparse array design for integrated sensing and communications," *IEEE Commun. Lett.*, vol. 28, no. 1, pp. 1–5, Jan. 2023.

[32] E. Grossi, M. Lops, and L. Venturino, "Energy efficiency optimization in radar-communication spectrum sharing," *IEEE Trans. Signal Process.*, vol. 69, pp. 3541–3554, May 2021.

[33] Y. Liu, S. Liu, X. Liu, Z. Liu, and T. S. Durrani, "Sensing fairness-based energy efficiency optimization for UAV enabled integrated sensing and communication," *IEEE Wireless Commun. Lett.*, vol. 12, no. 20, pp. 1702–1706, Oct. 2023.

[34] Q. Liu, R. Luo, H. Liang, and Q. Liu, "Energy-efficient joint computation offloading and resource allocation strategy for ISAC-aided 6G V2X networks," *IEEE Trans. Commun.*, vol. 7, no. 1, pp. 413–423, Mar. 2023.

[35] L. Chen, Z. Wang, Y. Du, Y. Chen, and F. R. Yu, "Generalized transceiver beamforming for DFRC with MIMO radar and MU-MIMO communication," *IEEE J. Sel. Areas Commun.*, vol. 40, no. 6, pp. 1795–1808, Jun. 2022.

[36] F. Liu, Y.-F. Liu, C. Masouros, A. Li, and Y. C. Eldar, "Cramér–Rao bound optimization for joint radar-communication beamforming," *IEEE Trans. Signal Process.*, vol. 70, pp. 240–253, 2022.

[37] Z. Qiu, K. Duan, Y. Wang, Z. Liao, and J. He, "Designing constant modulus approximate binary phase waveforms for multi-target detection in MIMO radar using LSTM networks," *IEEE Trans. Veh. Technol.*, vol. 20, no. 6, pp. 240–253, Feb. 2024.

[38] C. Tsinos, A. Arora, and Y. Yang, "Joint transmit waveform and receive filter design for dual-function radar-communication systems," *IEEE J. Sel. Topics. Signal. Process.*, vol. 15, no. 6, pp. 1378–1392, Nov. 2021.

[39] F. Dong and W. Wang, "Joint beamforming design for dual-functional MIMO radar and communication systems guaranteeing physical layer security," *IEEE Trans. Veh. Technol.*, vol. 7, no. 1, pp. 537–549, Jan. 2023.

[40] A. Liu et al., "A survey on fundamental limits of integrated sensing and communication," *IEEE Commun. Surv. Tuts.*, vol. 24, no. 2, pp. 994–1034, Apr.–Jun. 2022.

[41] N. Su, F. Liu, and C. Masouros, "Secure radar-communication systems with malicious targets: Integrating radar, communications and jamming functionalities," *IEEE Trans. Wireless Commun.*, vol. 20, no. 1, pp. 83–95, Jan. 2021.

[42] X. Qian, X. Hu, C. Liu, M. Peng, and C. Zhong, "Sensing-based beamforming design for joint performance enhancement of RIS-aided ISAC systems," *IEEE Trans. Commun.*, vol. 71, no. 11, pp. 6529–6545, Nov. 2023.

[43] D. Cong, S. Guo, S. Dang, and H. Zhang, "Vehicular behavior-aware beamforming design for integrated sensing and communication systems," *IEEE Trans. Intell. Transp. Syst.*, vol. 24, no. 6, pp. 5923–5935, Jun. 2023.

[44] P. Wang, Z. Yan, N. Wang, and K. Zeng, "Resource allocation optimization for secure multidevice wirelessly powered backscatter communication with artificial noise," *IEEE Trans. Wireless Commun.*, vol. 21, no. 9, pp. 7794–7809, Sep. 2022.

[45] Z. Dai, R. Li, J. Xu, Y. Zeng, and S. Jin, "Rate-region characterization and channel estimation for cell-free symbiotic radio communications," *IEEE Trans. Commun.*, vol. 71, no. 2, pp. 674–687, Feb. 2023.

[46] H. Zheng, C. Pan, and C. Zhang, "Robust transmission design for RIS-aided wireless communication with both imperfect CSI and transceiver hardware impairments," *IEEE Internet Things J.*, vol. 10, no. 5, pp. 4621–4635, Mar. 2023.

[47] D. W. K. Ng, E. S. Lo, and R. Schober, "Robust beamforming for secure communication in systems with wireless information and power transfer," *IEEE Trans. Wireless Commun.*, vol. 13, no. 8, pp. 4599–4615, Aug. 2014.

[48] M. Gao, J. Yang, H. Li, and Y. Wang, "Robust beamforming optimization design for RIS-aided MIMO systems with practical phase shift model and imperfect CSI," *IEEE Internet Things J.*, vol. 11, no. 1, pp. 958–973, Jan. 2024.

[49] Z. Yu, X. Hu, C. Liu, M. Peng, and C. Zhong, "Location sensing and beamforming design for IRS-enabled multi-user ISAC systems," *IEEE Internet Things J.*, vol. 70, no. 6, pp. 5178–5193, Nov. 2022.

[50] Y. Xu, S. Jiang, Q. Xue, X. Li, and C. Yuen, "Throughput maximization for NOMA-based cognitive backscatter communication networks with imperfect CSI," *IEEE Internet Things J.*, vol. 10, no. 22, pp. 19595–19606, Nov. 2023.

[51] K.-Y. Wang, A. M.-C. So, T.-H. Chang, W.-K. Ma, and C.-Y. Chi, "Outage constrained robust transmit optimization for multiuser MISO downlinks: Tractable approximations by conic optimization," *IEEE Trans. Signal Process.*, vol. 62, no. 21, pp. 5690–5705, Nov. 2014.

[52] Z. He, W. Xu, H. Shen, Y. Huang, and H. Xiao, "Energy efficient beamforming optimization for integrated sensing and communication," *IEEE Trans. Commun.*, vol. 11, no. 7, pp. 1374–1378, Jul. 2022.

[53] A. Bazzi, M. Chafii, and H. Guo, "On outage-based beamforming design for dual-functional radar-communication 6G systems," *IEEE Trans. Wireless Commun.*, vol. 22, no. 8, pp. 5598–5612, Aug. 2023.

[54] Z. Ren, L. Qiu, J. Xu, and D. W. K. Ng, "Robust transmit beamforming for secure integrated sensing and communication," *IEEE Trans. Commun.*, vol. 71, no. 9, pp. 5549–5564, Sep. 2023.


**Yongjun Xu** (Senior Member, IEEE) received the Ph.D. degree (Hons.) in communication and information system from Jilin University, Changchun, China, in 2015.

From December 2018 to December 2019, he was a Visiting Scholar with Utah State University, Logan, UT, USA. From 2021 to 2023, he was a Bayu Youth Scholar of Chongqing. He is currently a Full Professor with the School of Communications and Information Engineering, Chongqing University of Posts and Telecommunications, Chongqing, China. His recent research interests include symbiotic radio, RIS, ISAC, resource allocation, Internet of Things, and backscatter communications.

**Na Cao** received the B.Eng. degree in electronic information engineering from Henan Normal University, Xinxiang, China, in 2021. She is currently working toward the M.S. degree in communications and information engineering with the Chongqing University of Posts and Telecommunications, Chongqing, China.

Her research interests include integrated sensing and communications, and robust resource allocation.

**Yi Jin** received the B.S. degree in communication and information engineering from the Nanjing University of Information Science and Technology, Nanjing, China, in 2005, and the Ph.D. degree in communication and information engineering from Southeast University, Nanjing, in 2013.

He is currently with the China Academy of Space Technology, Xi'an, China. His research interests include communication signal processing, satellite communications, and networking.

**Haibo Zhang** received the Ph.D. degree in signal and information processing from the Beijing University of Posts and Telecommunications, Beijing, China, in 2013.

From 2015 to 2016, he was a Visiting Scholar with the Department of Electrical and Computer Engineering, North Carolina State University, Raleigh, NC, USA. He is currently an Associate Professor with the School of Communications and Information Engineering, Chongqing University of Posts and Telecommunications, Chongqing, China. His research interests include vehicle network and mobile edge computing.

**Chongwen Huang** (Member, IEEE) received the B.Sc. degree from Nankai University, Tianjin, China, in 2010, the M.Sc. degree from the University of Electronic Science and Technology of China, Chengdu, China, in 2013, and Ph.D. degree from the Singapore University of Technology and Design (SUTD), Singapore, in 2019, all in communications and information engineering.

From October 2019 to September 2020, he was a Postdoc with SUTD. Since September 2020, he joined with Zhejiang University as a tenure-track young Professor.

Dr. Huang was the recipient of 2021 IEEE Marconi Prize Paper Award, 2023 IEEE Fred W. Ellersick Prize Paper Award, and 2021 IEEE ComSoc Asia-Pacific Outstanding Young Researcher Award. His main research interests include holographic MIMO surface/RIS, B5G/6G wireless communications, mmWave/THz communications, and deep learning technologies for wireless communications.

**Qianbin Chen** (Senior Member, IEEE) received the Ph.D. degree in communication and information system from the University of Electronic Science and Technology of China, Chengdu, China, in 2002.

He is currently a Full Professor with the School of Communications and Information Engineering, Chongqing University of Posts and Telecommunications, Chongqing, China. His recent research interests include RIS, ISAC, resource allocation, and Internet of Things.

**Chau Yuen** (Fellow, IEEE) received the B.Eng. and Ph.D. degrees in electrical and electronics engineering from Nanyang Technological University, Singapore, in 2000 and 2004, respectively.

He was a Postdoctoral Fellow with Lucent Technologies Bell Labs, Murray Hill, NJ, USA, in 2005, and a Visiting Assistant Professor with The Hong Kong Polytechnic University, Hong Kong, in 2008. From 2006 to 2010, he was with the Institute for Infocomm Research, Singapore. From 2010 to 2023, he was with the Engineering Product Development Pillar, Singapore University of Technology and Design. Since 2023, he has been with the School of Electrical and Electronic Engineering, Nanyang Technological University. His research interests include green communications, integrated sensing and communications, and wireless power transfer.